Journal of Imaging Science and Technology® 63(6): 060410-1–060410-12, 2019.

Deep Image Demosaicing for Submicron Image Sensors

Irina Kim, Seongwook Song, Soonkeun Chang, Sukhwan Lim, and Kai Guo
S.LSI, Device Solutions, Samsung Electronics, 1-1, Samsungjeonja-ro, Hwaseong-si, Gyeonggi-do, Korea
E-mail: irina.s.kim@gmail.com

Abstract. *Latest trend in image sensor technology allowing submicron pixel size for high-end mobile devices comes at very high image resolutions and with irregularly sampled Quad Bayer color filter array (CFA). Sustaining image quality becomes a challenge for the image signal processor (ISP), namely for demosaicing. Inspired by the success of deep learning approach to standard Bayer demosaicing, we aim to investigate how artifacts-prone Quad Bayer array can benefit from it. We found that deeper networks are capable to improve image quality and reduce artifacts; however, deeper networks can be hardly deployed on mobile devices given very high image resolutions: 24MP, 36MP, 48MP. In this article, we propose an efficient end-to-end solution to bridge this gap—a duplex pyramid network (DPN). Deep hierarchical structure, residual learning, and linear feature map depth growth allow very large receptive field, yielding better details restoration and artifacts reduction, while staying computationally efficient. Experiments show that the proposed network outperforms state of the art for standard and Quad Bayer demosaicing. For the challenging Quad Bayer CFA, the proposed method reduces visual artifacts better than state-of-the-art deep networks including artifacts existing in conventional commercial solutions. While superior in image quality, it is 2–25 times faster than state-of-the-art deep neural networks and therefore feasible for deployment on mobile devices, paving the way for a new era of on-device deep ISPs.* © *2019 Society for Imaging Science and Technology.*
[DOI: 10.2352/J.ImagingSci.Technol.2019.63.6.060410]

1. INTRODUCTION

Most digital cameras capture color images using a single image sensor overlaid with a color filter array (CFA), acquiring only one color per pixel and therefore producing heavily subsampled raw image, which is further interpolated in the image signal processor (ISP) by the process called *demosaicing*. Despite of variety of available CFA patterns (RGBW, Fuji X-Trans, etc.), Bayer CFA remains "de facto" standard for most manufacturers for its simplicity and low cost [1]. Another underlying reason is that the majority of ISPs are manually designed and carefully tuned to process Bayer CFA, so significant effort is needed to redesign and retune those pipelines to support other CFA patterns. Nevertheless, *sub*μm image sensors adopted recently in many flagship smartphones use Quad Bayer CFA, where four pixels of one color are grouped in 2×2 cells (see Figure 1). These four pixels after averaging or so called *binning* allow increasing light sensitivity in low-light illumination conditions: *e.g.*, Samsung 0.8 μm sensors (ISOCELL Bright GD1, GM1) may achieve sensitivity equivalent to 1.6 μm. When four pixels are merged, Quad Bayer becomes regular Bayer CFA at quarter image resolution; therefore higher sensor resolutions are required: *e.g.*, GM1 sensor needs 48MP raw input image to have efficient 12MP output image resolution.

For full resolution image capture, we need to demosaic Quad Bayer CFA. Unlike original Bayer pattern, Quad Bayer pattern is non-uniformly sampled and thus more prone to aliasing than regular Bayer CFA, as shown in Section 3. Aliasing causes more visual artifacts in Quad Bayer CFA image. To improve image quality in Quad Bayer CFA case, we need more advanced demosaicing methods.

Deep learning approach to Bayer demosaicing has shown improvement in image quality and artifact reduction over conventional state of the art [2–6]. Inspired by this, we attempt to address a more challenging Tetracell demosaicing problem with deep convolutional neural networks (CNN). We aim to achieve competitive image quality targeting very high image resolutions: 24MP, 36MP, 48MP, bounded by inference time feasible after optimization for deployment on mobile neural processing unit (NPU) or other available on-device AI. This defines this work as an extremely challenging practical application, not a pure academic research.

Since this is the first work addressing Tetracell or Quad Bayer CFA demosaicing with deep learning approach to the best of our knowledge, we adopted and trained several renowned networks for Quad Bayer CFA. Inspired by Syu [6], we trained classical super-resolution networks: Super Resolution CNN (SRCNN) [7] and Very Deep Super Resolution network (VDSR) [8]. SRCNN produced unsatisfactory results (see Figures 3). When we trained VDSR for Quad Bayer, objective quality is improved, but visual artifacts remained.

Inspired by the success of ResNet [10], we decided to exploit power of residual learning. We adopted popular super-resolution residual network architecture Enhanced Deep Super Resolution Network (EDSR) [11], without batch normalization and scaling layers. We also removed pixel shuffler layer since it produced visible artifacts and used mosaiced full resolution input. Similar conclusion to use full resolution input was made by Tan [5], but for Bayer CFA. Our deep residual network based on EDSR baseline achieved better quality than Tan's demosaicing network at the same depth level 20; however on real captured Tetra images artifacts still remained.

Received July 15, 2019; accepted for publication Oct. 14, 2019; published online Dec. 17, 2019. Associate Editor: Dileepan Joseph.
1062-3701/2019/63(6)/060410/12/$25.00

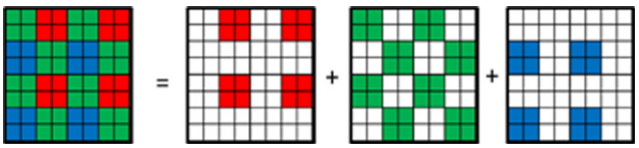

Figure 1. Tetracell or Quad Bayer color filter array decomposition into *R*, *G*, and *B* components.

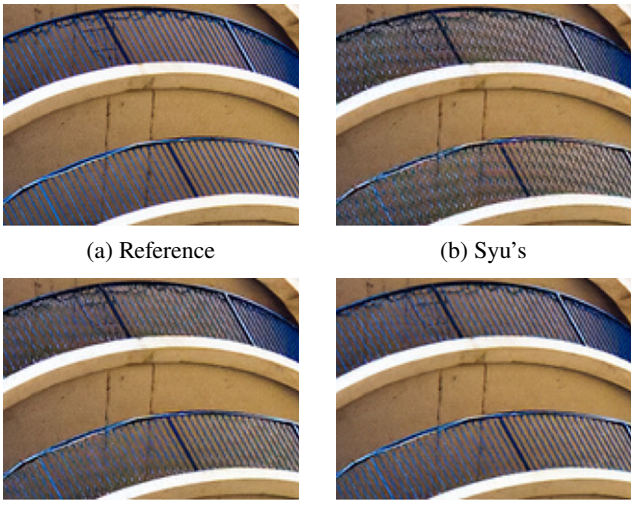

(a) Reference (b) Syu's

(c) Gharbi's (d) Ours (DPN)

Figure 2. We propose an efficient deep neural network architecture for demosaicing of Quad Bayer CFA adopted in submicron sensors. Trained on the same data, it outperforms state-of-the-art deep neural networks [2, 6] in terms of both objective and subjective quality. Example of improved color moiréartifact in image 100 from Urban100 dataset [9] is shown here. Zippering artifact removal is shown in Fig. 3.

Straightforward solution to improve quality is to increase network depth. Indeed increasing network depth level to level 30 yielded in better quality and helped to reduce artifacts. The problem with this approach was computational burden. For instance, to run inference for 48MP image we need more than 120 TOPs (Trillion OPerations), while best performing on-device Artifical Intelligence (AI) hardware can offer up to 7 TOPs. Recent approaches to network optimization can achieve up to 10 times speed-up. With reasonable budget x4 on network optimization, we need to design a network at least four times faster than EDSR.

In this article, we introduce a multi-resolution deep convolutional duplex pyramid network (DPN) for image demosaicing. We first build feature pyramid with several resolutions; then we reconstruct each feature map at the corresponding resolution level. Inspired by U-Net [12], we connect each pyramid level with skip connection. We exploit global and local residual learning that allow faster convergence addressing vanishing gradient problem. Finally, we propose to use linear feature growth instead of exponential. Deep hierarchical structure and slow feature map growth allow large receptive field, yielding better details restoration and artifacts reduction.

Experiments show that the proposed method outperforms both conventional and deep state of the art for Bayer

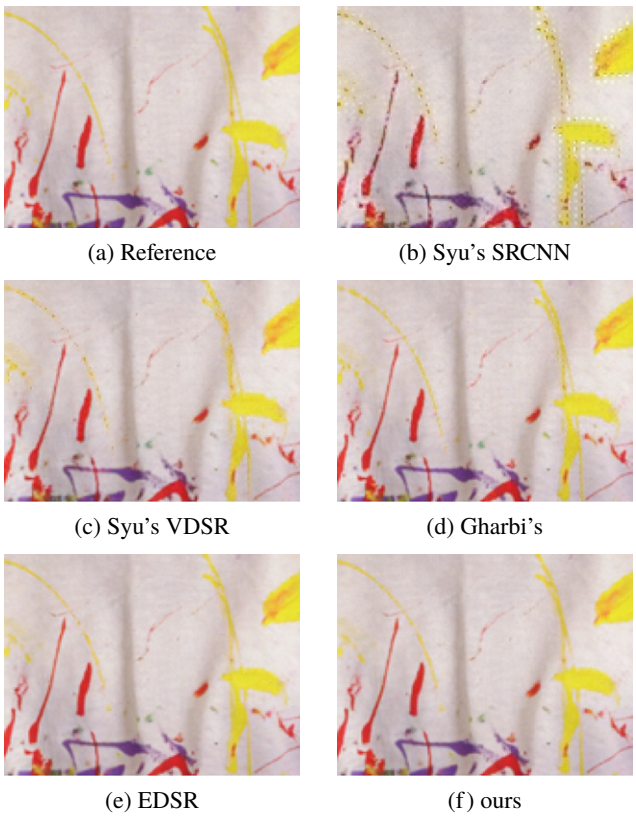

(a) Reference (b) Syu's SRCNN

(c) Syu's VDSR (d) Gharbi's

(e) EDSR (f) ours

Figure 3. Illustration of reduced zippering artifact (from image 5 in McMaster dataset): (a) Reference ground truth, (b) Syu's SRCNN, (c) Syu's VDSR, (d) Gharbi's, (e) EDSR, (f) ours (DPN).

CFA. For Tetracell CFA it outperforms existing networks both in image quality and complexity (see Table V and Figure 4). Being 4.3 times faster than EDSR and 25 times faster than Deep Recursive Residual Network (DRRN) [13], it outperforms state-of-the-art networks in image quality, surpassing 40dB for Kodak dataset [14].

To the best of our knowledge, this is the first work addressing a challenging demosaicing problem for new CFA patterns adopted in latest smartphones with a novel, generic deep learning solution using hierarchical network architecture. Proposed multi-resolution duplex pyramid network (DPN) with linear feature growth and residual learning, applied to recently adopted in submicron image sensors Quad Bayer CFA, could achieve an upper bound in image quality. Proposed efficient network outperformed state-of-the-art deep networks not only in image quality, but also in complexity. Being an order of magnitude faster, it enables a high quality image capture, at extremely high resolutions, on mobile devices.

2. RELATED WORKS

Demosaicing of each color channel can be treated as an interpolation problem and therefore can be solved with simple bilinear interpolation of corresponding missing color samples. While it is working well for one color channel or gray image producing blurred output without artifacts, it fails to produce good image quality for demosaicing

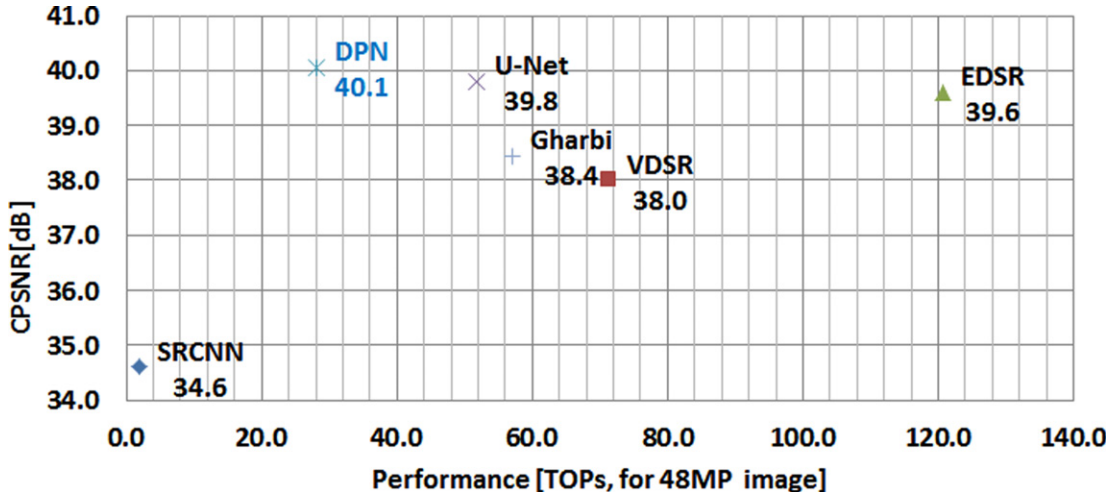

Figure 4. The proposed solution outperformed state-of-the-art deep networks in terms of inference speed: 2× faster than U-Net [12], 4.3× faster than EDSR [11], while being superior in image quality.

Table I. Duplex pyramid network configuration

Layer	FM1	FM2	FM3	FM4	FM5	FM6	FM7	FM8	FM9	FM10
#inputs	3	64	96	128	160	192	160	128	96	64
#outputs	64	96	128	160	192	160	128	96	64	64
Conv1	3 × 3	3 × 3	3 × 3	3 × 3	3 × 3	3 × 3	3 × 3	3 × 3	3 × 3	3 × 3
Conv2	3 × 3	3 × 3	3 × 3	3 × 3	3 × 3	3 × 3	3 × 3	3 × 3	3 × 3	3 × 3

Table II. Objective quality evaluation results for Tetracell demosaicing [CPSNR/SSIM]. Best results are marked in bold.

Dataset	Metric	SRCNN	VDSR	Gharbi	EDSR	U-Net	Proposed
Kodak	CPSNR	34.6	38.0	38.4	39.6	39.8	**40.1**
	SSIM	0.9577	0.9760	0.9811	0.9836	0.9842	**0.9846**
McM	CPSNR	32.4	35.6	36.8	37.5	37.5	**37.6**
	SSIM	0.9156	0.9503	0.9589	0.9637	0.9634	**0.9842**
Moire	CPSNR	30.2	32.6	34.0	35.4	35.6	**35.9**
	SSIM	0.9021	0.9280	0.9451	0.9542	0.9562	**0.9572**
HDR-VDP	CPSNR	27.8	30.2	31.4	32.4	32.3	**32.6**
	SSIM	0.9105	0.9407	0.9567	0.9643	0.9644	**0.9655**
Urban100	CPSNR	31.1	34.7	36.4	37.3	37.4	**37.7**
	SSIM	0.9491	0.9685	0.9762	0.9794	0.9796	**0.9799**

Table III. Comparison with the state of the art for Bayer CFA.

Method	CPSNR[dB], McM dataset	CPSNR[dB], Kodak dataset
Bilinear	32.5	32.9
Hirakawa [19]	33.8	36.1
Buades [24]	35.5	37.3
Zhang [22]	36.3	37.9
Klatzer [25]	30.8	35.3
Heide [26]	38.6	40.0
Tan [5]	37.5	40.4
Gharbi [2]	39.5	41.2
DPN (ours)	**39.5**	**42.3**

due to inter-channel dependency: severe zippering occurs along high frequency components, like edges and textures. Subsampling of color channels results in aliasing, producing more visually disturbing artifacts: color moiré, false colors, and maze artifacts.

Signal processing approach was extensively applied to the demosaicing problem over the past four decades [15, 16]. Early methods used the frequency approach to design aliasing-free filters [17]. Hand-crafted filters were designed to improve the zippering effect in early works [18]. To improve the performance near edges, median filtering of color differences was done in [19], gradient-based approach was also extensively used [20]. While many approaches use color differences, Monno proposed to use color residuals, by interpolating G channel first with bilinear interpolation followed by the improvement of red and blue color residuals [21]. Many successful methods use directional interpolation and inter-channel correlations [22], some exploit redundancy of natural images with non-local self-similarity and require heavy processing [23, 24]. For more thorough review, please refer to [15].

Table IV. Performance estimation [TOPs]. Best number is highlighted in bold.

Metric	SRCNN	VDSR	Gharbi	EDSR	DRRN	U-Net	DPN	DPN (lite)
Number of parameters	20,099	740,736	596,099	1,259,075	301,824	5,128,064	4,984,320	4,416,128
Performance for 48MP [TOPs]	1.9	71.3	57	120.8	708	51.8	28	12.5
Performance for 36MP [TOPs]	1.4	53.2	42.8	90.6	530.6	38.8	21	9.4
Performance for 24MP [TOPs]	1.0	35.6	28.5	60.4	353.8	25.9	14	6.3
Performance for 20MP [TOPs]	0.6	22.3	17.8	37.7	221	16.2	8.8	3.9
CPSNR on Kodak dataset [dB]	34.6	38.0	38.4	39.6	39.2	39.8	**40.1**	39.6

Table V. Ablation study effect on image quality.

Factor	CPSNR [dB]	Difference [dB]
Exponential depth growth	40.1	–
Linear depth growth	40.1	0.0
No global residual learning	39.7	0.4
Using residual skip connections	39.6	0.5

Nevertheless, conventional methods cannot achieve good image quality and often suffer from the visual artifacts. Moreover, the majority of signal processing methods are designed assuming certain CFA: mostly standard Bayer, sometimes Fuji X-Trans; thus they cannot be easily generalized to support other CFA. Edge direction orientation detection followed by filtering, usually exploited in modern demosaicing algorithms, and needs to be redesigned. Machine learning approaches were also applied recently to demosaicing; see work based on energy minimization [25] or full ISP modeling proposed by Heide [26]. Despite of being very expensive computation-wise, they failed to produce competitive image quality.

Deep learning based methods surpassing human recognition ability for computer vision have started to gain attention for low-level vision tasks as well in the last five years. From the pioneering work of Dong for super-resolution [7], many solutions were proposed, e.g., refer to the best performing methods [27]. We review works related to image demosaicing as follows.

First end-to-end solution for joint Bayer denoising and demosaicing was proposed by Gharbi [2]. Given a Bayer image, they extracted four RGGB channels and concatenated it with estimated noise channel. Those five channels served as a low-resolution input for CNN. They then used VDSR-like plain network architecture with stacked convolutions and global residual path. They also concatenated original mosaiced Bayer planes to upsampled feature maps before final convolution. Their main contribution is applying data-driven approach for demosaicing and publishing a new training dataset by hard patches mining using two metrics to detect artifacts-prone patches: HDR-VDP2 [28] and moiré detection metric using Fourier transform.

Several works were trying to exploit domain knowledge from conventional methods. For instance, multi-stage network architecture was proposed by Tan exploiting the idea of interpolating green channel first and then interpolating red/blue color differences guided by green channel, frequently used in conventional methods [4]. Domain knowledge was also used in two step deep learning approach in [29], suggesting feeding CNN with initially interpolated image by efficient low complexity conventional algorithms: improved bilinear with custom designed filters [18] or gradient-based algorithm [20] and then using multiple separate CNNs to refine color differences. Despite showing some improvement in CPSNR, their solution is complex and slow. Furthermore, it requires initial interpolation and separate training of multiple networks.

Super-resolution networks were adopted by Syu for Bayer and X-Trans demosaicing in [6]: SRCNN [7] and VDSR. Syu showed that deep VDSR outperformed shallow SRCNN. Tan proposed to use residual networks for joint demosaicing and denoising or demosaicing [5]. He used plain stacked residual block architecture with injected noise channel inspired by Gharbi's approach [2]. He tried depth 20 residual network and got marginal improvement over Gharbi's work with similar complexity. Kokkinos in [30] proposed to use the iterative method using popular denoising network DnCNN [31] to ease training procedure using a small amount of training samples, but it provided only marginal improvement, with longer inference time due to 5–10 iterations (3 times versus Gharbi's).

Fully convolutional networks were proposed by Long [32] for image segmentation, followed by its improved version with multi-scale features allowing capturing the context at various resolutions of U-Net [12]. U-Net, originally proposed for medical applications, has been successfully used in many segmentation tasks. Buggy tried several network architectures including U-net for image demosaicing [33]. He utilized RGGB channels as input achieving better result with U-Net than with [31] and ResNet [11]. He concluded that U-Net architectures perform better than DnCNN networks. There is no clear conclusion on residual networks in [33].

Plain encoder–decoder architecture with symmetric skip connections (RED-Net) was proposed by Mao in [34]. RED-Net used skip connections to connect encoder and decoder parts, but their network is plain, not multi-resolution. They tried various network depths including deeper network

with 30 layers (RED30). Performance of the deeper RED-Net was only marginally better than previous works.

A feature pyramid network (FPN) for object detection was proposed by Lin [35]. FPN constructs feature pyramid level by using feature maps from the network with lateral skip connections and 1×1 convolutions. The architecture of the FPN despite being somewhat similar to the DPN has different concept and purpose. It is not encoder–decoder architecture; on the contrary, constructed feature pyramid is used as input to other networks for region extraction.

3. QUAD BAYER CFA ANALYSIS

In this section, we show that Quad Bayer CFA has more aliasing than standard Bayer CFA. This aliasing induces more visual artifacts if we apply existing conventional demosaicing methods; therefore, more sophisticated methods are required to improve the image quality for Quad Bayer case.

To perform frequency analysis of the Quad Bayer CFA, we use frequency structure matrix approach [17]. The frequency structure represents the spectrum of the image filtered with CFA and it can be calculated using symbolic discrete Fourier transform (DFT).

For Bayer CFA we provide an example as follows. Without loss of generality, we assume GRBG order in this work.

Given Bayer CFA matrix H_{Bayer}:

$$H_{Bayer} = \begin{bmatrix} G & R \\ B & G \end{bmatrix}, \tag{1}$$

we can obtain the frequency structure matrix by applying symbolic DFT:

$$S_{Bayer} = DFT\left(H\|_{Bayer}\right) = \begin{bmatrix} FL & 2 \cdot FC_2 \\ -2 \cdot FC_2 & 2 \cdot FC_1 \end{bmatrix}, \tag{2}$$

where

$$FL = \frac{1}{4}\left(2G + R + B\right), \tag{3}$$

$$FC_1 = \frac{1}{8}\left(2G - R - B\right), \tag{4}$$

$$FC_2 = \frac{1}{8}\left(B - R\right). \tag{5}$$

We can see that S_{Bayer} has one luminance and three chrominance components at $\left(0, \frac{\pi}{2}\right), \left(\frac{\pi}{2}, 0\right) \wedge \left(\frac{\pi}{2}, \frac{\pi}{2}\right)$.

We calculate the frequency structure for Tetra CFA denoted as S_{Tetra} in a similar fashion as follows.

Using Quad Bayer CFA matrix H_{Tetra}:

$$H_{Tetra} = \begin{bmatrix} G & G & R & R \\ G & G & R & R \\ B & B & G & G \\ B & B & G & G \end{bmatrix}, \tag{6}$$

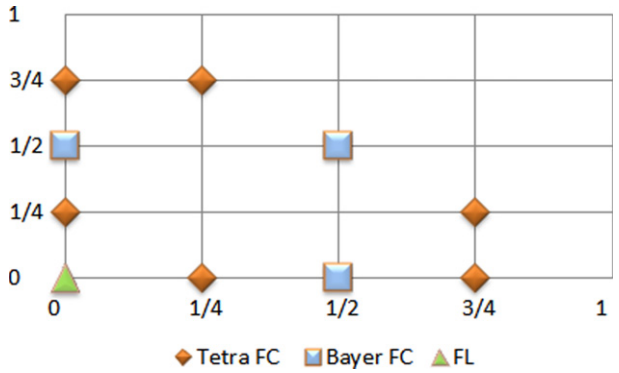

Figure 5. Frequency components of Quad Bayer and regular Bayer CFAs.

we can obtain the frequency structure matrix for Tetracell CFA as follows:

$$S_{Tetra} = \begin{bmatrix} FL & FC_2 & 0 & FC_2 \\ -FC_2 & 0 & 0 & FC_1 \\ 0 & 0 & 0 & 0 \\ -FC_2 & 0 & 0 & 0 \end{bmatrix}. \tag{7}$$

Figure 5 shows location of frequency components of Quad Bayer and regular Bayer CFAs. We can see that Tetra or Quad Bayer CFA has six color components at different locations compared to Bayer with only three different color components. It proves that Quad Bayer CFA is more prone to aliasing than standard Bayer CFA.

4. PROPOSED METHOD

In our work, we use the following commonly used linear observation image model:

$$Y = M * X + \mu, \tag{8}$$

where $Y \in R^n$ is an observed raw image from the sensor, $X \in R^{3n}$ is a reconstructed RGB image, $M \in R^{n \times 3n}$ is a degradation matrix, $\mu \in R^n$ is a noise vector, and n is the number of measurements.

Image demosaicing is an inverse and ill-posed problem. Solving it with traditional methods would be expensive. Instead, we directly learn end-to-end mapping function F from training sample pairs by taking sRGB images as ground truth and mosaiced images as observed images. We then estimate model parameters Ω by minimizing Euclidean L_2 function.

$$L_2\left(\Omega\right) = \frac{1}{n}\sum_{i=1}^{n}\left\|F\left(X_i, \Omega\right) - Y_i\right\|_2^2. \tag{9}$$

We propose an end-to-end generic solution that can be applied to an arbitrary sized input image. We model CFA pattern with distortion operator M, so our solution can be applied to arbitrary CFA pattern of any size, including Bayer, Tetra, Kodak and Canon RGBW, Fuji X-Trans, etc. We first describe the proposed network architecture followed by proposed changes from previous works.

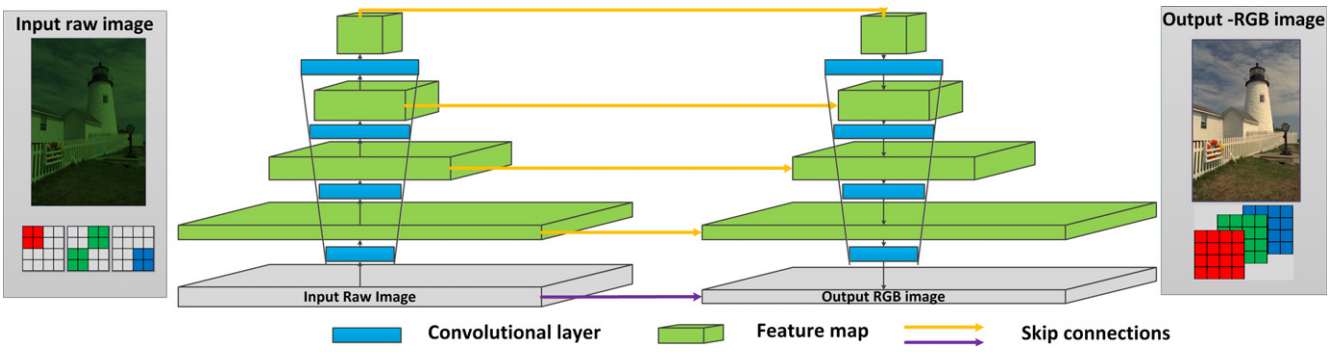

Figure 6. Duplex pyramid network: feature pyramids.

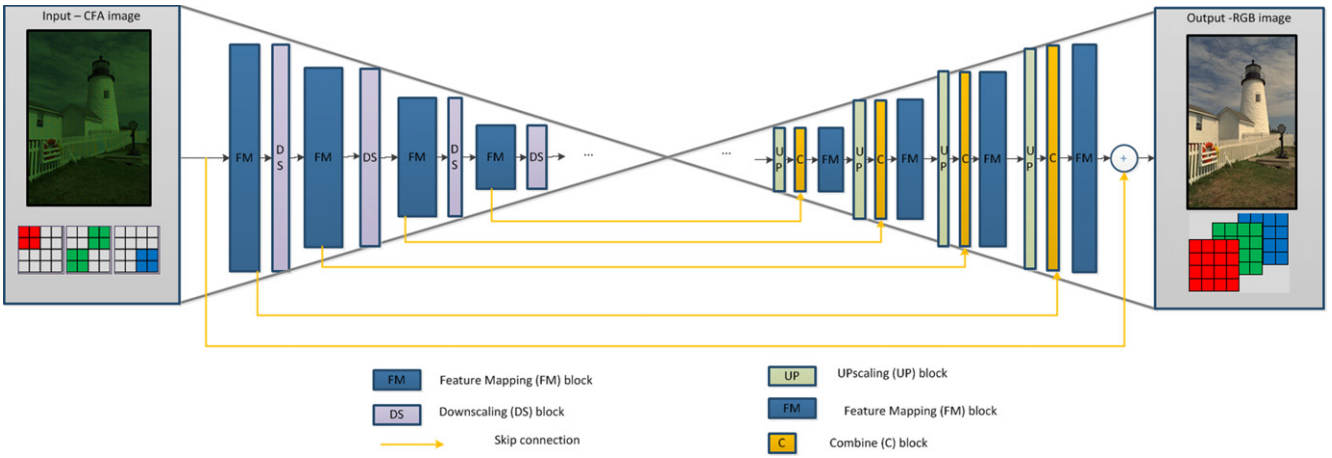

Figure 7. Block diagram of the proposed neural network.

4.1 *Network Architecture*

The network consists of two connected feature map pyramids: feature extraction (FE) pyramid and feature reconstruction (FR) pyramid (see Figure 6), so we name it duplex pyramid network (DPN).

FE pyramid consists of feature mapping (FM) and downscaling (DS) blocks, at each resolution level. FR pyramid is built with UPscaling (UP), combine (C), and feature mapping (FM) blocks as depicted in Figure 7. Downscaling block performs subsampling with learned 3×3 kernels. Upscaling block in our network incarnation performs learned upscaling. We use transposed convolution with (2×2) kernel in UP block and strided convolution (3×3) in DS block. Note that we do not use pooling in our network. Combine block performs either concatenation or addition of two inputs. In the particular incarnation of the proposed network, we use concatenations of map channels or dense skip connection. Feature mapping block consists of several stacked convolutions as depicted in Figure 8.

4.2 *Residual Learning*

Inspired by the success of ResNet by He [10], we exploit residual learning in our work. We use global residual learning with skip connection and forward input to output signal as shown in Fig. 6. Starting from global residual learning, we further use residual learning at each resolution level. Inspired by U-Net, we use skip dense connections with combine block. Finally we use local residual learning in feature mapping block depicted in Fig. 8. Residual block was inspired from SRResNet [36]. In the current network configuration, we remove batch normalization and use only one convolution in the residual part.

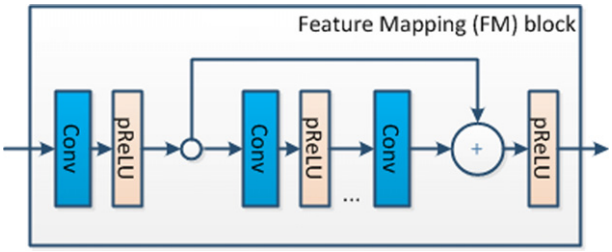

Figure 8. Block diagram of the feature mapping (FM) block.

4.3 *Non-exponential Feature Map Growth*

Many network architectures use exponential function (2^x), where x is the current resolution level, to increase the number of feature map channels in the next level. This design choice is often used in vision problems, starting from classical VGG network, where the number of feature channels is doubled after pooling, to compensate for the associated loss [37]. In practice, exponential growth of feature map depth d

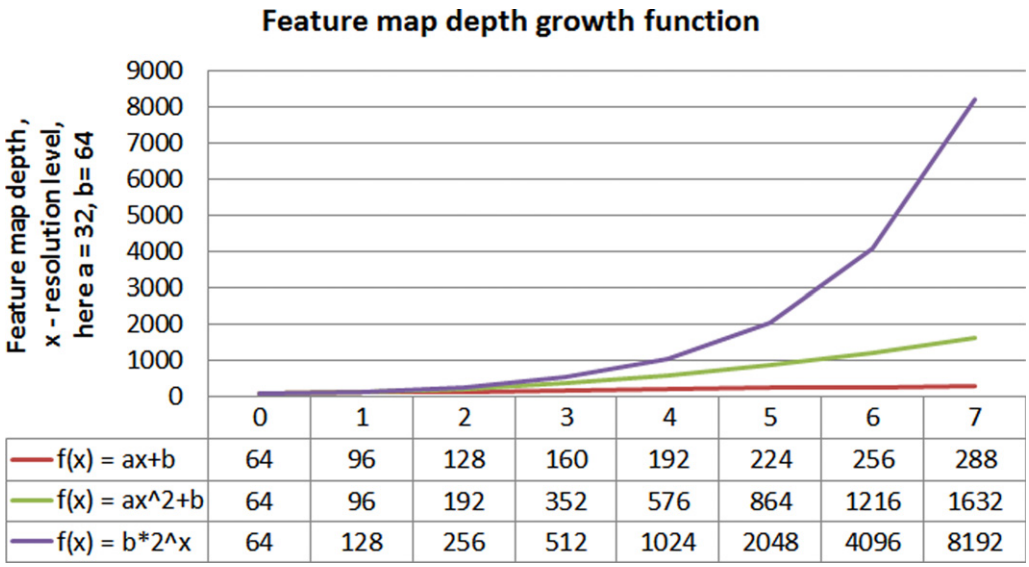

	0	1	2	3	4	5	6	7
f(x) = ax+b	64	96	128	160	192	224	256	288
f(x) = ax^2+b	64	96	192	352	576	864	1216	1632
f(x) = b*2^x	64	128	256	512	1024	2048	4096	8192

Figure 9. Feature map depth growth function: exponential versus linear.

leads to huge number of parameters when going deeper with resolution scale. To increase receptive field, we need to increase depth and resolution levels; however, for mobile applications with limited memory constraint, it becomes unfeasible: for instance, U-Net with five levels has 82 million parameters.

Indeed, for image processing applications, networks like VGG seem to be heavily over-parameterized, so some works succeed to largely reduce the number of parameters, up to 50 times [38]. If so, why do not we reduce the number of parameters in network, before doing optimization?

In this work, instead of using exponential function for feature map growth we propose to use a monotonically increasing function as long as it has smaller growth rate. Exact function shape and parameters can be selected to meet requirements for specific application (linear, log, polynomial, etc.).

For low-level imaging problems like demosaicing, we propose to use a linear function:

$$f(x) = ax + b, \tag{10}$$

where x is the resolution level, b is the initial feature map size, and a is the growth rate.

We suggest the practical rule of thumb for selecting lower bound of growth coefficient a:

$$a \geq b/2. \tag{11}$$

The proposed linear function with $b = 64$, $a = 32$ is shown in Figure 9. Experiments with this setting allow increasing resolution up to level 5 with affordable number of parameters and performance.

5. EXPERIMENTS

In this section, we describe reference networks and provide training details.

5.1 *Reference Networks Details*

We provide details of several networks we trained to produce reference for Tetra CFA demosaicing. First we trained classical super-resolution networks SRCNN and VDSR. We adopted SRCNN and VDSR architectures as is. For residual network EDSR, we adopted single scale baseline EDSR. We removed upsampling block (pixel shuffler) from the original EDSR, because it produced visually disturbing artifacts, and processed image at full resolution.

In order to reduce memory and bandwidth we tried to use recursive architecture DRRN [13]. We trained network with one residual block, with 25 iterations. With only two convolutional layers it is very compact in terms of memory and shows good results in terms of artifacts reduction. However, it had lower CPSNR despite of using wider feature maps (128). Furthermore, DRRN can be difficult to use it due to performance issue (inference time is multiplied by the number of recursions).

For U-Net, we used original architecture except that each map was padded to keep original image resolution, we also removed last layer used for segmentation. We also pad image size after each convolution. In this article, we present results of U-Net with two levels, with 5 million parameters.

5.2 *Proposed Network Details*

Using concepts described in Section 3, we used following incarnation of the duplex pyramid network in this work. With total five resolution levels, we use same feature mapping block (FM) with two convolutions across all resolutions. The number of input/output channels changes with the proposed linear growth function across the resolution levels as shown in Table I. We use minimum kernel size 3 and stride 1 in all FM blocks across all resolution levels and parametric RELU (pRELU) as the activation function.

5.3 *Datasets*

Training data is a key to success. In this work, we use the training dataset provided by Gharbi [2]. The dataset consists of 2.6 million of training samples from IMAGENET.

We evaluate objective image quality on public datasets widely used in image restoration tasks: Kodak [14], McMaster [22], and Urban100 datasets [9]. We also report the performance on Moiré and HDR-VDP datasets designed to check the performance of the algorithm on artifacts-prone images (each containing one thousand samples) provided in [2]. We also used captured raw 16MP Tetra CFA images with challenging scenes such as resolution and Siemens star charts, to evaluate subjective image quality.

5.4 *Training Details*

We trained each network from scratch using sRGB image patches of size 128×128 as ground truth and mosaiced patches as input. We did not use any initial interpolation to mosaic patches, but used zero filling of each R/G/B plane. We augmented input data with random flip and rotation and random crop when possible.

We trained all our models with ADAM optimizer [39] with the following settings: $\beta_1 = 0.9 = 0.999$, $\varepsilon = 10^{-8}$, weight decay $= 10^{-8}$. We set initial learning rate as 10^{-4} and schedule learning rate decrease at milestones [3, 10, 20], with decay $= 0.1$. We used L_2 loss in all our experiments, for the sake of fair comparison.

Same training data was used for all trained networks. None of the networks we trained was fine-tuned or used additional training data, in order to provide reference benchmark. This means that the performance of each network reported here can be further improved. All models were implemented using Pytorch and trained on NVIDIA Titan X GPUs.

6. RESULTS

6.1 *Image Quality Evaluation*

We provide objective evaluation results of all trained networks on public datasets in Table II. We used following standard datasets: Kodak, McMaster [22], HDR-VDP, Moiré [2], and Urban100 in our tests. To evaluate image quality, we use standard widely used image metrics: CPSNR (Color Peak-to-Signal Noise Ratio) [16], SSIM (Structural SIM index) [40]. The proposed network outperforms other methods on all standard benchmarks in terms of objective image quality using both CPSNR and SSIM metrics.

Subjective evaluation shows significant reduction of major demosaicing artifacts: color moiré and false colors (see Figures 11–13 for more details). For example, we provide an example of best performing networks: EDSR, U-Net, and DPN in Figure 2. You can see that our solution is significantly better in removing large scale moiré patterns due to large receptive field. Better edges and thin lines restoration can be also observed in Figs. 11–13. Zippering artifact inherent to many conventional methods can be removed by using deeper network. For instance, severe zippering can be observed when using shallow SRCNN, which is improved by using deeper VDSR and completely removed by deeper networks (see Fig. 11).

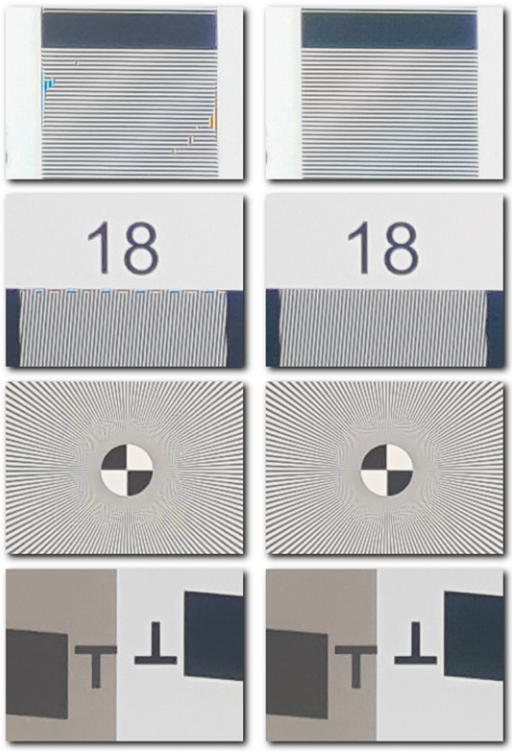

Figure 10. Artifacts mitigation on real Tetracell raw images: left—conventional, right—proposed.

6.2 *Evaluation on Real Tetracell Dataset*

We evaluated our method on real captured raw Tetra images. We ran inference with trained weights on white balanced raw Quad Bayer image. After that the image was processed with the ISP simulator. We compared against conventional algorithm implemented in Samsung mobile phone and observed improvement in sharpness, color moiré, edges and texture preservation. With the proposed method, we could achieve significant reduction of visual artifacts as shown in Figure 10.

6.3 *Comparison with the State of the Art*

We present the performance of the proposed solution versus state of the art for Bayer CFA demosaicing in this section. CPSNR values for McMaster and Kodak dataset are given in Table III. Our network retrained for Bayer CFA outperforms both conventional and deep methods exceeding 42 dB, while being orders of magnitude faster. In case of McMaster dataset, we got similar CPSNR values, but subjective visual tests showed better artifacts reduction. For instance, the example from McMaster dataset shows improved zippering artifacts compared to Gharbi's in Fig. 2. Note that some papers also reported values with 42dB CPSNR, but when we trained them with the same settings, results were up to 2dB worse than reported, so we did not put unconfirmed results in the table.

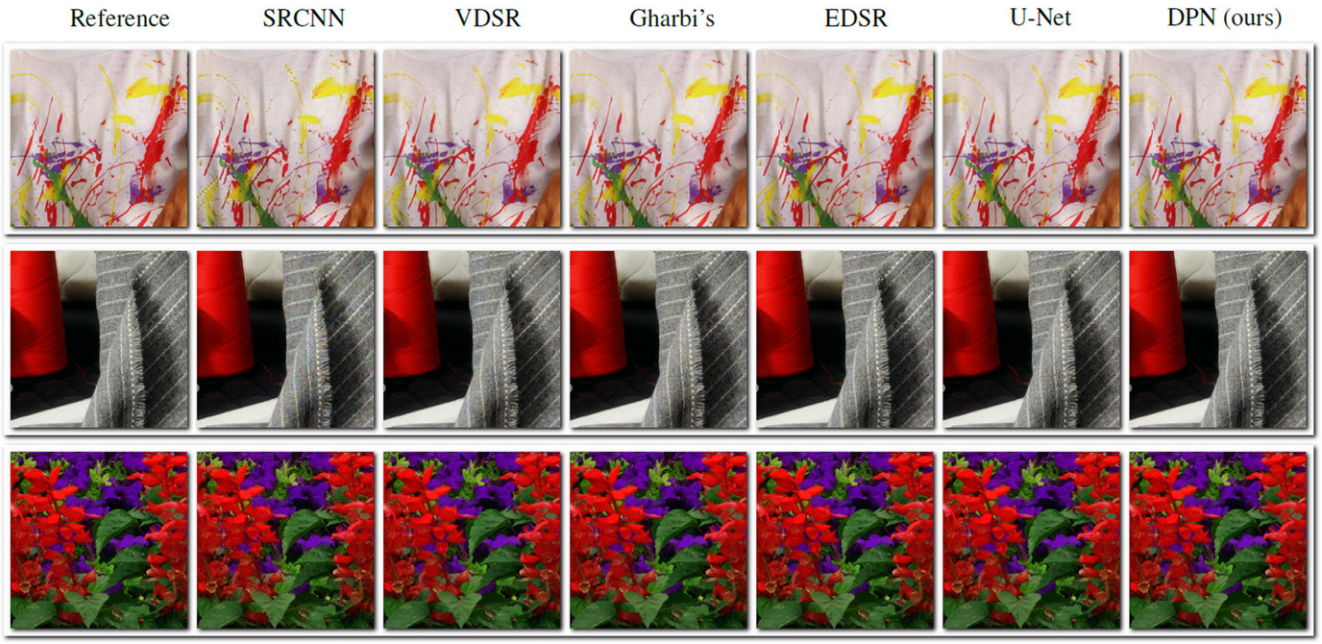

Figure 11. Image quality evaluation results on McMaster dataset [22]: no zippering, improved moiré and details restoration (images 5,7,17).

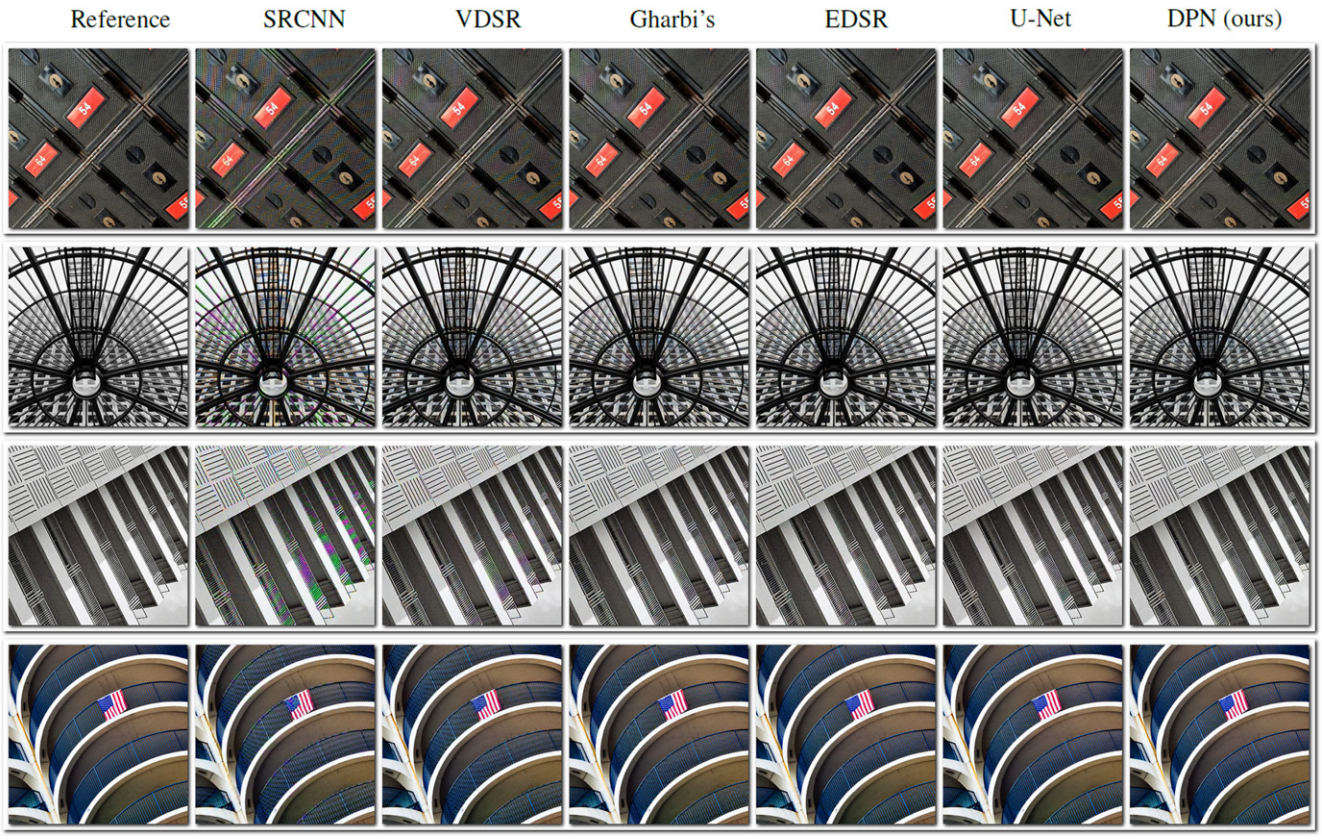

Figure 12. Image quality evaluation results on Urban100 dataset [9]: improved moiré and false colors (images 6,72,92,100).

6.4 *Performance Estimation*

We estimate the performance for still image capture scenario, when we need to reconstruct full resolution image, in Table IV. Apparently, the proposed DPN is the best in terms of quality while being 2 times faster than U-Net, 4.3 times faster than EDSR and 25 times faster than DRRN. Note that

Figure 13. Image quality evaluation results on Moire dataset [8]: improved color moire and false colors versus state-of-the-art (images 19, 158, 166, 182, 209, 334).

we trained lite version of DPN with removed concatenations. This incarnation of the network is twice faster but has slightly lower CPSNR. Both networks are feasible for deployment on mobile devices after optimization.

6.5 *Ablation Study*

To check degradation that may be caused by linear feature depth growth, we trained DPN with exponential feature map growth. However, we did not observe improvement in quality: we got CPSNR 40dB on Kodak dataset despite of 13.5 times more parameters. This is aligned with our hypothesis that CNNs with exponential feature map growth are over-parameterized for low-level vision applications. We also performed ablation study to understand the effect of each improvement point. We removed global residual learning and kept other network structures same, and we also reverted residual skip connections from dense skip connections, i.e., have only summation instead of concatenations. Results are summarized in Table IV. We can conclude that combination of features contributed to the final network performance.

6.6 *Fusion with Conventional Algorithms*

Deep learning (DL) methods proved to be superior to conventional methods in terms of details preservation, moirë, and other visually disturbing artifacts reduction. If we analyze the image, we can see that this is usually critical on high frequency areas of the image containing edges, because limited filter sizes of 5×5–21×21 often fail to detect correct edge orientation. In homogeneous areas, conventional low complexity algorithms perform well.

Based on these observations, we propose to fuse DL output with conventional algorithm output only on areas with high frequency details prone to artifacts. If we use this approach, we can run network inference only in some regions of interest. For natural images, artifacts-prone area is relatively small, for difficult images like resolution charts we can detect up to 1/4 of the image area so that inference time budget can be increased four times. This approach is particularly beneficial when we have hardware demosaicing in ISP, since we can perform DL and conventional demosaicing in parallel. Visual image quality can be significantly improved by using this approach with relaxed conditions for CNN inference performance.

7. DISCUSSION

All networks were tested on real Tetracell raw data in linear domain and show good generalization ability despite of being trained on sRGB data. Raw image needs to be white balanced before applying deep neural network, in a similar fashion as for conventional demosaicing algorithms. Unlike conventional demosaicing, neural network does not change raw image noise profile which is beneficial for pipelines using denoising after demosaicing.

An interesting point is that experimental results show 2dB difference in CPSNR on the same dataset when using same network on Bayer CFA and Quad Bayer CFA. Despite of having same input data dimensions, non-uniform sampling leads to more aliasing as shown in Section 3. To achieve similar image quality for Tetracell image, we need deeper or more sophisticated networks.

7.1 *Limitations*

There is one limitation to input image size associated with downscaling. Input image width and height should be a multiple of 2^{L+1}, where L is the resolution level. In real applications, this condition normally holds. If not, image should be padded or cropped to satisfy above condition.

7.2 *Extensions*

Proposed network architecture can be used for any CFA pattern including Nona, RGBW, Fuji X-trans, etc. By modeling the mosaic operator, we can get distorted images for any pattern for training. By adding noise channel to current network as in [2], we can extend it to solve denoising or joint demosaicing and denoising problem. In general, it can be applied to any image restoration problem including but not limited to image super-resolution, inpainting, etc.

8. CONCLUSION

In this article, we introduced a challenging problem of demosaicing of Tetracell or Quad Bayer CFA adopted in the latest submicron image sensors. We show that conventional approaches from standard Bayer demosaicing fail to reduce artifacts observed in Quad Bayer CFA. We found that deeper convolutional networks can improve image quality, but can be hardly deployed on mobile devices due to complexity.

We proposed an efficient multi-resolution residual network architecture with slow growing feature maps that outperforms state-of-the-art deep neural network architectures and conventional methods in Quad Bayer CFA demosaicing, while staying computationally efficient.

The proposed network can be used for any CFA pattern. Originally designed for more challenging Tetra CFA demosaicing, it outperforms state of the art for both regular Bayer CFA and Quad Bayer CFA. Tested on real captured images with mobile camera with Quad Bayer CFA, it is superior to conventional commercial solutions and can significantly reduce visual artifacts inherent to demosaicing.

The proposed solution not only provides superior image quality, but is also computationally efficient due to its multi-resolution structure and slow growing features and therefore feasible for deployment on mobile devices with embedded AI accelerators (DSP, GPU, NPUs) or other available hardware.

REFERENCES

[1] B. Bruce, "Color imaging array," Patent 7 (1976).
[2] M. Gharbi, G. Chaurasia, S. Paris, and F. Durand, "Deep joint demosaicking and denoising," ACM Trans. Graph. **35**, 191:1–191:12 (2016).
[3] D. Khashabi, S. Nowozin, J. Jancsary, and A. W. Fitzgibbon, "Joint demosaicing and denoising via learned nonparametric random fields," IEEE Trans. Image Process. **23**, 4968–4981 (2014).
[4] R. Tan, K. Zhang, W. Zuo, and L. Zhang, "Color image demosaicking via deep residual learning," *Proc. IEEE Int'l. Conf. on Multimedia and Expo (ICME)* (IEEE, Piscataway, NJ, 2017).
[5] H. Tan, H. Xiao, S. Lai, Y. Liu, and M. Zhang, "Deep residual learning for image demosaicing and blind denoising," Elsevier Pattern Recognit. Lett. **8** (2018).
[6] N.-S. Syu, Y.-S. Chen, and Y.-Y. Chuang, "Learning deep convolutional networks for demosaicing," CoRR abs/1802.03769.2018.
[7] C. Dong, C. C. Loy, K. He, and X. Tang, "Image super-resolution using deep convolutional networks," IEEE Trans. Pattern Anal. Mach. Intell. **38**, 295–307 (2016).
[8] J. Kim, J. K. Lee, and K. M. Lee, "Accurate image super-resolution using very deep convolutional networks," *Proc. IEEE Conf. on Computer Vision and Pattern Recognition (CVPR)* (IEEE, Piscataway, NJ, 2016).
[9] J.-B. Huang, A. Singh, and N. Ahuja, "Single image super-resolution from transformed self-exemplars," *Proc. IEEE Conf. on Computer Vision and Pattern Recognition (CVPR)* (IEEE, Piscataway, NJ, 2015).
[10] K. He, X. Zhang, S. Ren, and J. Sun, "Deep residual learning for image recognition," *Proc. IEEE Conf. on Computer Vision and Pattern Recognition (CVPR)* (IEEE, Piscataway, NJ, 2016).
[11] B. Lim, S. Son, H. Kim, S. Nah, and K. M. Lee, "Enhanced deep residual networks for single image super-resolution," *Proc. IEEE Conf. on Computer Vision and Pattern Recognition (CVPR) Workshops* (IEEE, Piscataway, NJ, 2017).
[12] O. Ronneberger, P. Fischer, and T. Brox, "U-Net: Convolutional networks for biomedical image segmentation," *Medical Image Computing and Computer-Assisted Intervention (MICCAI)* (Springer, Cham, Switzerland, 2015).

[13] Y. Tai, J. Yang, and X. Liu, "Image super-resolution via deep recursive residual network," *Proc. IEEE Computer Vision and Pattern Recognition (CVPR)* (IEEE, Piscataway, NJ, 2017).
[14] A. Loui, J. Luo, S.-F. Chang, D. Ellis, W. Jiang, L. Kennedy, K. Lee, and A. Yanagawa, "Kodak's consumer video benchmark data set: concept definition and annotation," *Proc. Int'l. Workshop on Workshop on Multimedia Information Retrieval* (ACM, New York, NY, 2007).
[15] X. Li, B. Gunturk, and L. Zhang, "Image demosaicing: A systematic survey," Proc. SPIE **6822** (2008).
[16] D. Menon and G. Calvagno, "Color image demosaicking: An overview," Sig. Proc. Image Comm. **26**, 518–533 (2011).
[17] D. Alleysson, S. Süsstrunk, and J. Hérault, "Linear demosaicing inspired by the human," IEEE Trans. Image Process. **14**, 439–449 (2005).
[18] R. Malvar and R. Cutler, "High-quality linear interpolation for demosaicing of bayer-patterned color images," *Proc. Int'l. Conf. of Acoustic, Speech, and Signal Processing (ICASSP)* (IEEE, Piscataway, NJ, 2004).
[19] K. Hirakawa and T. W. Parks, "Adaptive homogeneity-directed demosaicing algorithm," IEEE Trans. Image Process. **14**, 360–369 (2005).
[20] I. Pekkucuksen and Y. Altunbasak, "Gradient based threshold free color filter array interpolation," *Proc. Int'l. Conf. on Image Processing (ICIP)* (IEEE, Piscataway, NJ, 2010).
[21] Y. Monno, D. Kiku, M. Tanaka, and M. Okutomi, "Adaptive residual interpolation for color image demosaicking," *Proc. IEEE Int'l. Conf. on Image Processing (ICIP)* (IEEE, Piscataway, NJ, 2015).
[22] L. Zhang, X. Wu, A. Buades, and X. Li, "Color demosaicking by local directional interpolation and nonlocal adaptive thresholding," J. Electron. Imaging **20**, 68221–68225 (2011).
[23] K. Chang, P. Lun Kevin Ding, and B. Li, "Color image demosaicking using inter-channel correlation and nonlocal self-similarity," Signal Process., Image Commun. **39**, 10 (2015).
[24] A. Buades, B. Coll, J.-M. Morel, and C. Sbert, "Self-similarity driven color demosaicking," IEEE Trans. Image Process. **18**, 1192–1202 (2009).
[25] T. Klatzer, K. Hammernik, P. Knobelreiter, and T. Pock, "Learning joint demosaicing and denoising based on sequential energy minimization," *Proc. IEEE Int'l. Conf. on Computational Photography (ICCP)* (IEEE, Piscataway, NJ, 2016).
[26] F. Heide, M. Steinberger, Y.-T. Tsai, M. Rouf, D. Pajak, D. Reddy, O. Gallo, J. Liu, W. Heidrich, K. Egiazarian, J. Kautz, and K. Pulli, "FlexISP: A flexible camera image processing framework," ACM Trans. Graph. **33**, 231:1–231:13 (2014).
[27] R. Timofte, E. Agustsson, L. V. Gool, M. Yang, L. Zhang, B. Lim, S. Son, H. Kim, S. Nah, K. M. Lee, X. Wang, Y. Tian, K. Yu, Y. Zhang, S. Wu, C. Dong, L. Lin, Y. Qiao, C. C. Loy, W. Bae, J. Yoo, Y. Han, J. C. Ye, J. Choi, M. Kim, Y. Fan, J. Yu, W. Han, D. Liu, H. Yu, Z. Wang, H. Shi, X. Wang, T. S. Huang, Y. Chen, K. Zhang, W. Zuo, Z. Tang, L. Luo, S. Li, M. Fu, L. Cao, W. Heng, G. Bui, T. Le, Y. Duan, D. Tao, R. Wang, X. Lin, J. Pang, J. Xu, Y. Zhao, X. Xu, J. Pan, D. Sun, Y. Zhang, X. Song, Y. Dai, X. Qin, X. Huynh, T. Guo, H. S. Mousavi, T. H. Vu, V. Monga, C. Cruz, K. Egiazarian, V. Katkovnik, R. Mehta, A. K. Jain, A. Agarwalla, C. V. S. Praveen, R. Zhou, H. Wen, C. Zhu, Z. Xia, Z. Wang, and Q. Guo, "NTIRE 2017 challenge on single image super-resolution: methods and results," *Proc. IEEE Conf. on Computer Vision and Pattern Recognition Workshops (CVPRW)* (IEEE, Piscataway, NJ, 2017).
[28] R. Mantiuk, K. Kim, A. Rempel, and W. Heidrich, "HDR-VDP-2: A calibrated visual metric for visibility and quality predictions in all luminance conditions," ACM Trans. Graph. **30**, 40:1–40:14 (2011).
[29] D. S. Tan, W. Chen, and K. Hua, "Deep demosaicking: adaptive image demosaicking via multiple deep fully convolutional networks,," IEEE Trans. Image Process. **27**, 2408–2419 (2018).
[30] F. Kokkinos and S. Lefkimmiatis, "Iterative joint image demosaicking and denoising using a residual denoising network," IEEE Trans. Image Process. **28**, 4177–4188 (2019).
[31] K. Zhang, W. Zuo, Y. Chen, D. Meng, and L. Zhang, "Beyond a gaussian denoiser: residual learning of deep CNN for image denoising," IEEE Trans. Image Process. **26**, 3142–3155 (2017).
[32] J. Long, E. Shelhamer, and T. Darrell, "Fully convolutional networks for semantic segmentation," *Proc. IEEE Conf. on Computer Vision and Pattern Recognition (CVPR)* (IEEE, Piscataway, NJ, 2015).
[33] R. Buggy, M. Forte, and F. Pitié, "Neural net architectures for image demosaicing," Proc. SPIE **10752** (2018).
[34] X.-J. Mao, C. Shen, and Y.-B. Yang, "Image restoration using very deep convolutional encoder-decoder networks with symmetric skip connections," *Proc. Advances in Neural Information Processing Systems* (Curran Associates Inc., Red Hook, NY, 2016).
[35] T.-Y. Lin, P. Dollar, R. Girshick, K. He, B. Hariharan, and S. Belongie, "Feature pyramid networks for object detection," *Proc. IEEE Conf. on Computer Vision and Pattern Recognition (CVPR)* (IEEE, Piscataway, NJ, 2017).
[36] C. Ledig, L. Theis, F. Huszár, J. Caballero, A. Cunningham, A. Acosta, A. Aitken, A. Tejani, J. Totz, Z. Wang, and W. Shi, "Photo-realistic single image super-resolution using a generative adversarial network," *Proc. IEEE Conf. on Computer Vision and Pattern Recognition (CVPR)* (IEEE, Piscataway, NJ, 2017).
[37] K. Simonyan and A. Zisserman, "Very deep convolutional networks for large-scale image recognition," (2014).
[38] A. Canziani, A. Paszke, and E. Culurciello, "An analysis of deep neural network models for practical applications," CoRR, abs/1605.07678 (2016).
[39] D.-P. Kingma and J. Ba, "Adam: A method for stochastic optimization." (2015).
[40] Z. Wang, A. Bovik, H. Sheikh, and E. Simoncelli, "Image quality assessment: from error visibility to structural similarity," IEEE Trans. Image Process. **13**, 600–612 (2004).